ACS OMEGA

Article

Cite This: ACS Omega 2018, 3, 6540−6545

Bias-Dependent Scanning Tunneling Microscopy Signature of Bridging-Oxygen Vacancies on Rutile TiO_2(110)

Willie B. Maddox,[†] Danda P. Acharya,[‡] G. Jeremy Leong,[†] Peter Sutter,[§] and Cristian V. Ciobanu*[,†]

[†]Department of Mechanical Engineering, Colorado School of Mines, 1500 Illinois Street, Golden, Colorado 80401, United States

[‡]Global Foundries, 400 Stone Break Extension, Malta, New York 12020, United States

[§]Department of Electrical and Computer Engineering, University of Nebraska-Lincoln, P.O. Box 880511, Lincoln, Nebraska 68588, United States

ABSTRACT: The rutile TiO_2(110) surface has long-served as a well-characterized, prototypical transition-metal oxide surface used in heterogeneous catalysis and photocatalytic water splitting. Naturally occurring defects on this surface, called bridging-oxygen (BO) vacancies, are important as they determine the overall reactivity of the surface. Herein, we report a bias-dependent, scanning tunneling microscopy (STM) signature of the BO vacancies on TiO_2(110): for sample bias voltages past a threshold of +3 V, the bright vacancies are flanked on either side (along the oxygen row) by two dark spots approximately shaped like half-moons. The BO vacancies have a bright aspect below the threshold bias also but are not surrounded by half-moon dark depressions. Using generalized gradient approximation calculations with Hubbard correction (GGA + U) for projected density of states (DOS) and simulated STM images, we find that the bias-dependent STM signature originates from (i) local DOS maxima of all BOs (lighter background that occurs above the threshold bias) and (ii) the increased separation between the first and second BO atoms neighboring the vacancy which leads to an apparent dip between these neighboring oxygens. These results offer a new striking example of the STM signature that appears without switching the polarity of the bias. Similar approaches can be employed for seeking distinguishing features on the surfaces of other large band gap semiconductors and insulators.

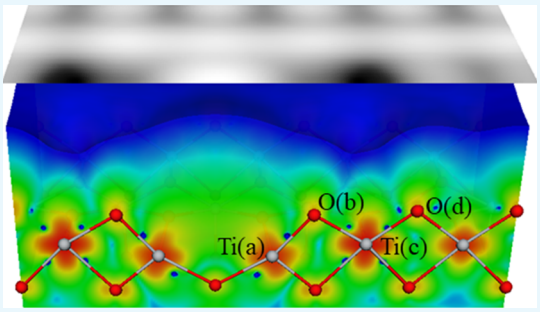

1. INTRODUCTION

Titanium dioxide is a prototypical transition-metal oxide widely used in photocatalysis,[1,2] heterogeneous catalysis,[3] as well as in solar[4,5] and sensing technologies.[6] Its most stable rutile TiO_2 surface, (110), is a de facto playground for fundamental investigations of reactivity of metal-oxide surfaces.[7−10] The stoichiometric TiO_2(110) exposes 5-fold coordinated Ti atoms, bridging oxygens (BOs), and 4-fold coordinated oxygens.[7] However, the surface is rarely stoichiometric, as it contains naturally occurring BO vacancies.[7,11] These vacancies, whose coverage can be controlled by ion sputtering and annealing, are important reactive sites for various adsorbates,[1,7,11,12] and therefore critically affect most chemical reactions occurring on the TiO_2 surface. The BO vacancies may effectively change the electronic structure of the surface, acting as electronic donors.[7] Scanning tunneling microscopy (STM) emerged as a key means to determine reaction intermediates on the surface, and, furthermore to give insight into the specific catalytic role played by this surface.[7,10−12] Using STM and density functional theory (DFT) simulation approaches, the BO vacancies have been differentiated from various adsorbates on the surface after some initial confusion over their individual signatures.[7,13−18] Over the last few decades, empty- and filled-state STM images (corresponding to opposite bias polarity) have been used to seek distinguishing features of electronic properties of surfaces,[19,20] of various reconstructions,[21,22] or adsorbate structures.[23,24] For example, contrast reversal is often associated with polarity changes for surfaces with semiconducting behavior.[19,20]

In this article, we show that BO vacancies have an STM "fingerprint" that occurs without changing the bias polarity, only its value: this signature is the presence of two dark, half-moon-shaped spots flanking the BO vacancy along the BO row, appearing when the positive sample bias voltage exceeds +3.0 V. The dark spots are not observable below this threshold bias. An unintended consequence of activating such a high threshold could be that (some) adsorbates desorb from the surface during scanning, thereby leaving only or mostly BO vacancies; if this desorption effect becomes undesirable, it could be controlled by lowering the tunneling current in STM imaging. Using DFT calculations in the framework of generalized gradient approximation (GGA) with the Hubbard correction (+U), and DFT-simulated STM images, we identify the origin of this BO vacancy fingerprint in STM. Specifically, we find that for bias voltages past a threshold, the oxygen rows

Received: May 30, 2018
Accepted: June 7, 2018
Published: June 18, 2018

DOI: 10.1021/acsomega.8b01056
ACS Omega 2018, 3, 6540−6545

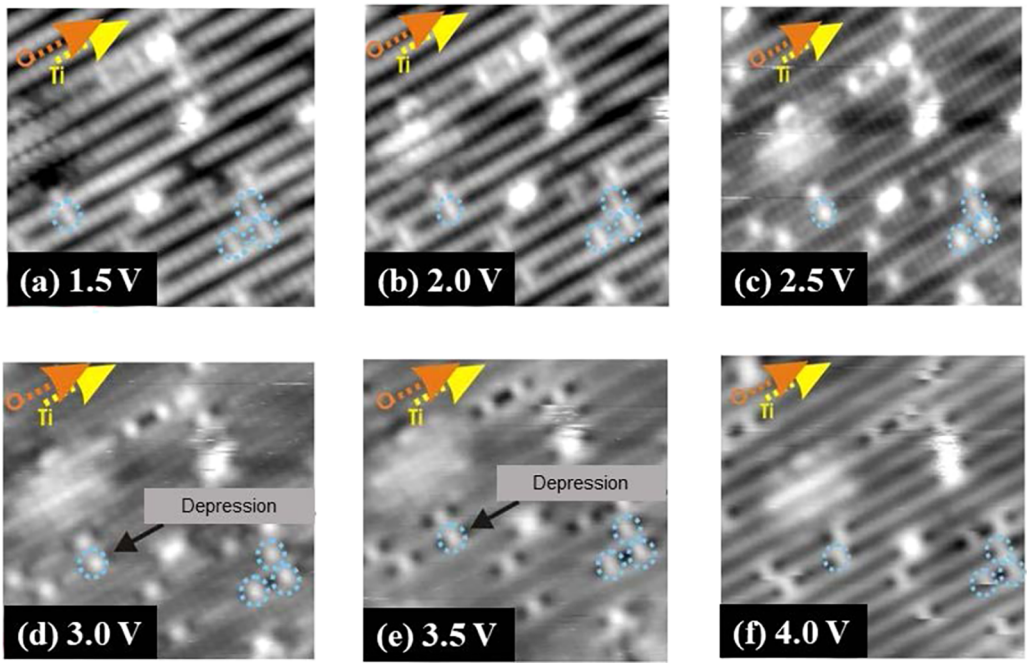

Figure 1. (a–f) Empty-state STM images of BO vacancies on the rutile $TiO_2(110)$ surface for sample bias voltages from (a) 1.5 to (f) 4.0 V, at a tunneling current I = 1.3 nA. The O and Ti rows are shown by the orange and yellow arrows, respectively. Below a threshold of 3.0 V, the bright BO vacancies are surrounded by diffuse bright areas, whereas for voltages above the threshold, we observe half-moon-shaped dark spots (depressions) situated along the BO row, on either side of the vacancies. There are four vacancies circled by blue dashed lines, whose apparent height profiles are analyzed in Figure 3.

become brighter and create contrast for the depressed surface 6-fold coordinated Ti atoms that are closest to the vacancy. These results offer a new striking example of the STM signature that appears without changing the polarity of the bias but simply increasing it gradually until (potentially) new STM features appear: as such, similar approaches can be employed for analyzing distinguishing features on the surfaces of other large band gap semiconductors and insulators.

2. METHODS

2.1. Experimental Details. $TiO_2(110)$ single-crystal samples (obtained from Princeton Scientific and Commercial Crystal Laboratories) were subjected to argon-ion sputtering cycles, followed by annealing at ∼910 K; the thermally reduced samples were subsequently cooled rapidly below 100 K, so as to retain a significant population of BO vacancies on the surface.[25,26] These vacancies were imaged using an ultrahigh vacuum (UHV) cryogenic STM system (Createc), operating at a temperature of 77 K and a pressure below 10^{-11} Torr, in the constant current mode with positive sample bias ranging from 1.0 to 4.0 V. Similar to other works,[25−27] we have used electrochemically etched tungsten tips, annealed by electron bombardment in UHV.

2.2. Computational Details. To investigate the electronic structure and the STM images of rutile $TiO_2(110)$ surfaces with single vacancies, we have carried out DFT calculations in the framework of the spin-dependent GGA, with the Perdew–Burke–Ernzerhof exchange–correlation functional[28] as implemented in the Vienna Ab Initio Software Package.[29−31] We have modified the Hamiltonian by adding a Hubbard correction U on the Ti d-states to prevent spurious delocalized solutions.[32] We use a value of U = 4.5 eV, which was reported to lead to midgap states for BO vacancies,[33] which is consistent with experimental findings.[34] We have used projector-augmented pseudopotentials,[31] a 500 eV plane-wave energy cutoff, and a 2 × 2 × 1 Γ-centered grid for sampling the Brillouin zone during structure relaxations. The slab structures in our simulations have 2 × 5 surface unit cells with dimensions of $2(a\sqrt{2}) = 13.20593$ Å and $5c = 14.85000$ Å along the $[1\bar{1}0]$ and the [001] directions, respectively. The slabs have 15 Å of vacuum and five O–Ti–O trilayers total, with one BO atom removed from the upper and lower surfaces. The middle trilayer is kept fixed, but all other atoms are relaxed until the residual forces are smaller than 0.025 eV/Å. After the structural relaxations, (partial) density of states (DOS) calculations were performed and used for simulations of STM images via the Tersoff–Hamman approach.[35]

3. RESULTS

Figure 1 shows STM images obtained for a sequence of bias voltages from 1.5 to 4.0 V, for the same tunneling current of 1.3 nA. When inspecting scans performed at different biases, we note that vacancies may sometimes hop along the BO row, but this effect is rare and rapid, that is, it is not significant on the time scale of the scan. At positive tunneling bias values, the Ti rows on the rutile $TiO_2(110)$ surface appear bright, while the O rows are dark; this is consistent with other experimental reports[8,9] for the row assignments on this surface. At low bias voltages, each oxygen vacancy appears as a bright spot with a diffuse halo around it (Figure 1a–c). However, as the bias voltage is increased past 3.0 V, dark spots with a half-moon shape surround the vacancies (Figure 1d–f). This is a distinct, bias-dependent signature of the BO vacancy, which has been overlooked in previous reports, typically using low biases (below the 3.0 V threshold identified here).[10,14] The origin of this STM signature of the oxygen vacancy has not been investigated so far, and we are analyzing it here based on DFT calculations compared with the experimental STM images.

DOI: 10.1021/acsomega.8b01056
ACS Omega 2018, 3, 6540−6545

We now describe the DFT calculations at the level of GGA + U aimed at elucidating the origin of the bias-dependent, half-moon depressions around the BO vacancies. GGA + U is deemed to be a good compromise between the tractability of the calculations and retaining a qualitatively correct description of the midgap states pointed out in other works.[14,33,34,36,37] The drawback is that at this level of theory, the band gap itself is still ∼1 eV smaller than in experiments,[33] which should reflect in a correspondingly smaller threshold for the emergence of half-moon depressions in the STM simulations (Figure 2). Indeed, Figure 2 shows that the dark depressions in

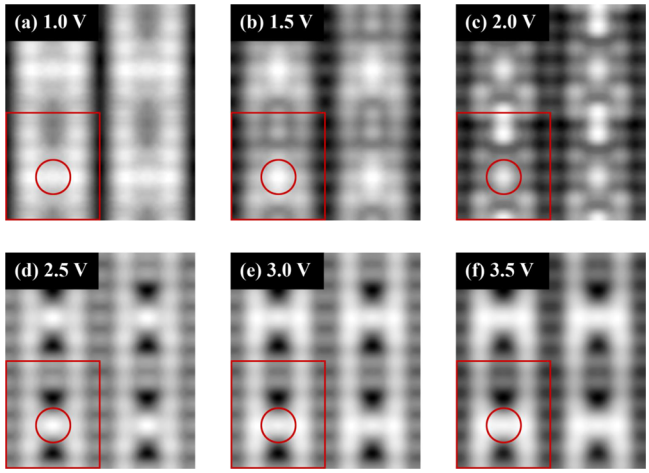

Figure 2. DFT-simulated empty-state STM images. For voltages below 2.0 V, there are no depressions around the vacancy [panels (a–c)]. For higher voltages, two dark spots appear along the BO row located about 1.4c away from the center of the vacancy [panels (d–f)]. Each panel shows a 2 × 5 surface cell (solid red box) with a vacancy (red circle); for clarity, this cell is repeated four times in the plane of the surface.

simulations start to appear at a bias of 2.0 eV, instead of the experimental value of 3.0 V. Regardless of whether a vacancy hops or not during STM scanning, its structure before and after the jump remains the same; hence, simulations of the STM images of a static BO vacancy in the unit cell are relevant for comparisons with experiments. The simulated and experimental STM images of the single BO vacancy are similar to each other (Figures 1 and 2). We have further analyzed the simulated and experimental images of the BO vacancies in terms of their apparent height on the surface. Figure 3 shows the height profiles along the BO rows for the four vacancies marked in Figure 1, and the corresponding profile from the DFT simulations of our 2 × 5 reduced TiO_2(110) supercells. For easy comparison, the height profiles were centered on the vacancy in all cases. As seen in Figure 3, all the curves (experimental and simulated) show the same locations of the depressions around the vacancy. The contrasts of the simulated and experimental STM images are different (Figure 3), which is likely due to the fact that the STM simulations shown in Figure 2 are based on computed DOS and do not include any tip effects.

This robust presence of the apparent depressions around vacancies above a certain threshold bias (2.0 V in the DFT simulations) suggests that the GGA + U approach can be used as a means to determine the physical origin of the bias dependence observed in experiments. Toward this goal, we start by calculating and plotting the DOS for the d-states of all

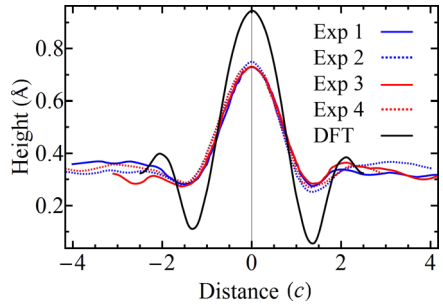

Figure 3. Apparent height profiles (red and blue curves) for the four BO vacancies marked by dashed circles in Figure 1 and the corresponding profile from the DFT simulations of a vacancy in a 2 × 5 surface cell (black curve). For easy comparison, all apparent height curves have been centered with their maximum on the exact location of the vacancy. All curves correspond to a bias voltage of 4.0 V and show similar locations of the depressions around the vacancy (1.4c–1.6c).

Ti atoms and the p-states of all O atoms in the simulation cell. The DOS plots are depicted in Figure 4 and show that there is

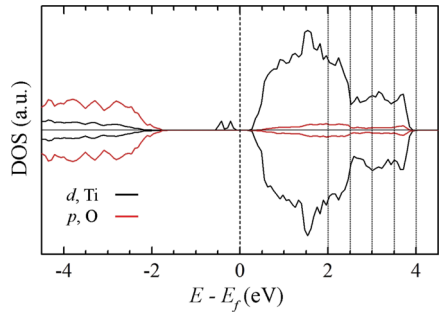

Figure 4. Calculated DOS for the d states of all Ti atoms and all O atoms (p states only) in the supercell. The two spin polarizations are shown as curves above and below the horizontal axis.

only one dominant peak for the d-states of Ti atoms past the DFT threshold of 2.0 V. The DFT-simulated STM images include states within a desired bias voltage range above the Fermi level; hence, the peak between 2.0 and 2.5 V is included for simulations in Figure 2d–f, all performed for a bias greater than 2.0 V.

Next, we focus on identifying which particular atoms in the simulation cell are responsible for the DOS peak between 2.0 and 2.5 V shown in Figure 4. We investigate the atoms that are near the BO vacancy, specifically the 5-fold coordinated atoms at the vacancy (a), the BO to which it is bonded (b), the next Ti atom (c) along the oxygen row, and the bridge-O atom (d) located two sites away from the vacancy. These atoms are shown in the inset of Figure 5a. The site-projected DOS in Figure 5 shows that the most pronounced peak occurs for the Ti (c) atoms in the 2–2.5 V range, while the 5-fold Ti (a) atoms have more maxima of similar strength in a wider bias range. The O (b) and O (d) atoms range also have clear maxima between 2 and 2.5 V (Figure 5). With this identification of the atoms responsible for the DOS peak between 2.0 and 2.5 V, we perform angular momentum projections of the DOS associated with Ti (c).

Figure 6a shows the angular momentum-projected d-states of this atom. The most pronounced DOS maximum occurs for the d_z^2 state of Ti(c), which has a lobe along the surface

DOI: 10.1021/acsomega.8b01056
ACS Omega 2018, 3, 6540–6545

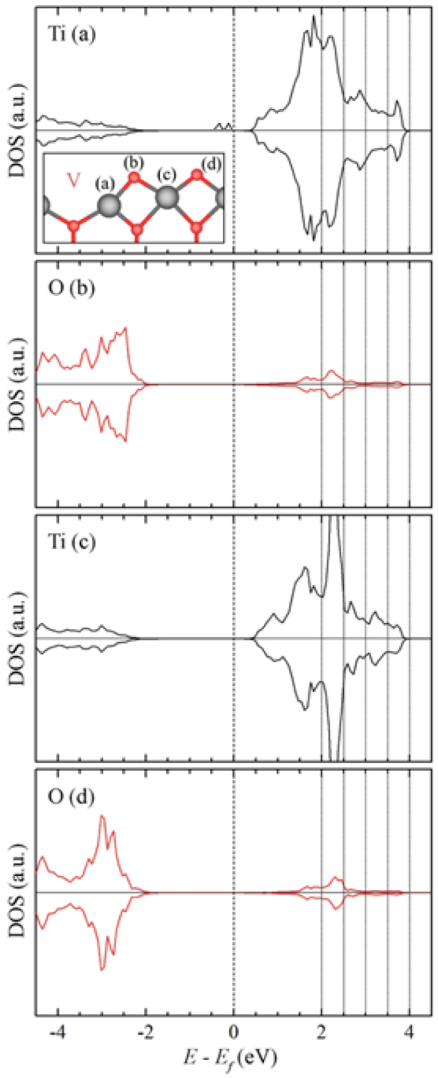

Figure 5. (a−d) Site-projected DOS for selected atoms along the BO row. Inset: (a) 5-fold coordinated Ti, (c) 6-fold coordinated Ti, and two BOs (b,d). Only d (p) states are included for the Ti (O) atoms. Ti (c), O (b), and O (d) have peaks between 2.0 and 2.5 V, which ultimately lead to the observed depressions around the vacancy, enabled by geometric relaxation effects that increase the separation between O (b) and O (d).

normal z and hence should lead to a bright spot strictly above the Ti (c) atom situated 1.5c away from the vacancy. However, instead of a bright spot, there is a dark half-moon-shaped spot at ∼1.4c away from the center of the vacancy, that is, just above the Ti (c) atom (Figures 2 and 3). This seeming contradiction can be understood by plotting concomitantly the simulated STM image and the charge density associated with all atoms and all angular momenta for the bias range of 2−2.5 V (Figure 6b). Figure 6b reveals that even though there is indeed a local maximum of the charge density above Ti (c) (associated mainly with d_z^2, Figure 6a), this maximum is not so pronounced as to overcome the fact that the Ti (c) atom lies ∼1.34 Å lower than the O (b) and O (d) oxygens at the surface. One may wonder why there is no such pronounced apparent dip in the STM images between any other BOs that are next to each other on the surface: the reason is that the distance between O (b) and O (d) is larger (due to asymmetric relaxation toward the vacancy, see inset in Figure

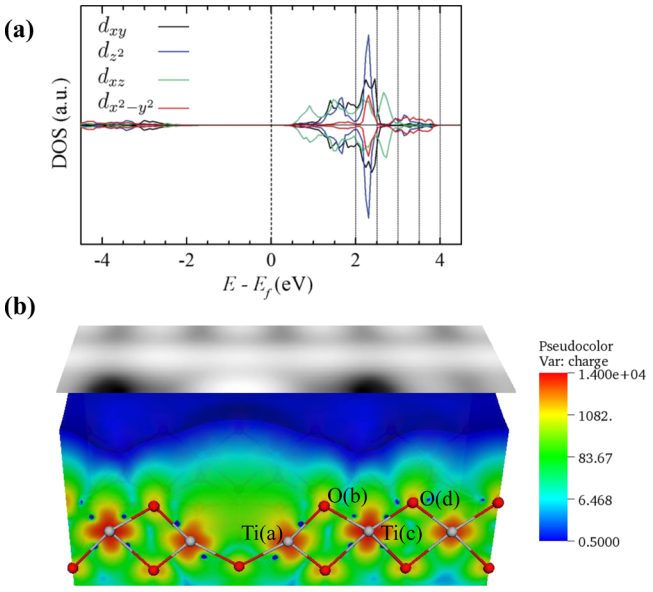

Figure 6. (a) Angular momentum-projected d-states corresponding to the 6-fold coordinated Ti that is closest to the vacancy along the BO row [atom Ti (c)]. The d_{yz} projection is small and omitted for clarity. (b) Spatial charge density (arbitrary units) corresponding to the states (all atoms, all angular momenta) in the 2.0−2.5 V energy window above the Fermi level. In this window, the pronounced maxima localized above the vacancy and above two BO atoms (c and 2c away from the vacancy) on one side of it lead to the dark spot above Ti (c).

5) than the nominal value between two neighboring BO on the stoichiometric surface, thus "allowing" the STM tip to record a sharper and wider dip between them (Figure 6b).

4. DISCUSSION

Below the threshold voltage, the Ti (a) atom has extended maxima, while the O atoms (b,d) do not have significant DOS maxima that would contribute strongly to the STM image (Figure 5); therefore, the dark half-moon spots would not appear below the threshold (Figures 1 and 2). To confirm this, we plot simulated STM images using only certain voltage windows that do not necessarily start from the Fermi level. These simulations are not meant to correspond to experiments the way those in Figure 2 do, but rather to isolate the contributions of different energy windows below and above the threshold level of 2.0 V. Indeed, below the 2.0 V threshold, there are no pronounced depressions (Figure 7a). The dark half-moon spots mainly originate from states in the 2−2.5 V window (Figure 7b), and, to a smaller extent, from states

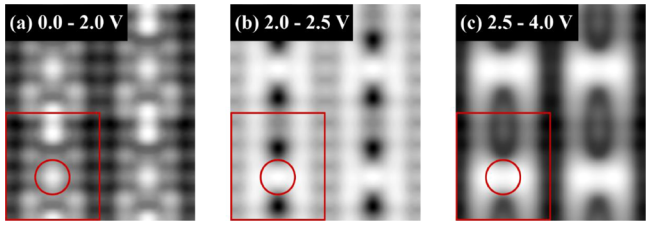

Figure 7. Simulated empty-state STM images obtained from states for selected bias intervals. The half-moon depressions show clearly for the 2.0−2.5 V window. The 2.5−4 V window also leads to depressions but with significantly lower contrast corresponding to the smaller density of Ti d states at biases beyond 2.5 V (Figure 4).

DOI: 10.1021/acsomega.8b01056
ACS Omega 2018, 3, 6540−6545

beyond this energy window (Figure 7c). An important aspect contributing to the appearance of dark depressions just above Ti (c) (Figure 6b) is that the BO rows become brighter when p states within 2−2.5 V are sampled (Figure 7b), hence creating contrast for the half-moon dark spots above Ti (c). This is borne out in experiments as well, where we see the oxygen rows "light up" when the bias is past the experimental threshold (compare, e.g., Figure 1a with 1d). The results in Figure 7 also indicate that the midgap states[14] do not contribute to the half-moon depressions (dark spots) around the vacancy; this is easily understood because the "responsible" bias window of 2.0−2.5 V is completely within the conduction band.

The results presented in Figure 1a−c are consistent with numerous other reports in the literature that show bright Ti rows, dark BO rows, and bright BO vacancies in STM at positive biases of 1−2 V.[8−10,18] In addition, we carried out STM scans at larger bias voltages, up to 4 V: this is how we uncovered the hallmark, half-moon depressions that flank the BO vacancies. Analysis of the projected DOS has shown that the bias-dependent STM signature originates from DOS maxima of the 5-fold coordinated Ti atoms next to the vacancy and two BO atoms on each side of it. As bias-dependent threshold behavior is investigated for a BO vacancy or adsorbate on the surface, it is important to check at the same time for the possible desorption of various species on the surface. For example, STM scans carried out at sample bias >3 V would desorb H atoms from the surface,[8,38] but would not affect too much the native BO vacancies which may only undergo sporadic hops along the BO row. In cases where desorption of an adsorbate requires a minimal dose of tunneling electrons (i.e., is controlled by the electron flux/current rather than the energy), the desorption (of H, or of other adsorbates) can be suppressed by lowering the tunneling current. An investigation of the multiple species on the surface with (sufficiently) different desorption biases and/or different thresholds for the onset of adsorbate-specific STM signatures may be useful. Another interesting aspect for future work is the study of bias-dependent STM signatures for large adsorbates that potentially allow for spanning wide bias intervals without desorption.

5. CONCLUSIONS

In conclusion, we have reported a bias-dependent STM signature for BO vacancies on the well-studied TiO_2(110) surface: for positive sample bias voltages above +3.0 V in experiments (or 2.0 V in GGA + U calculations), half-moon-shaped apparent depressions appear along the oxygen row at ∼1.4c away from the center of the vacancy. By studying the DOS projected on angular momentum components for selected atoms, we found that the origin of this characteristic STM signature of the BO vacancy is a high density of d states for the 5-fold coordinated Ti atoms at the vacancy and of p states for the O atoms around the vacancy (c and 2c away): this high DOS occurs primarily in the 3−3.5 V bias interval (2−2.5 V in GGA + U simulations). Although there is a local DOS maximum at the 6-fold coordinated surface Ti closest to the vacancy, this Ti lies sufficiently below the BO atoms that it appears dark despite the local d_z^2 DOS maximum. Midgap states do not contribute to the reported bias-dependent STM signature.

The current results on bias-dependent signature of defects on the surface are expected to contribute in cases where there is potential ambiguity in distinguishing different adsorbates and/or defects on surfaces. For example, in the past, there has been some confusion between the signature of hydroxyls (OH) and vacancies on TiO_2(110):[13] while this was resolved by studying, comparatively, DFT simulations and experimental STM images in terms of line profiles through images,[8,10,15] our results suggest that another way to differentiate between various adsorbates (or between adsorbates and vacancies) could be scanning at higher bias voltages where one can take advantage of characteristic bias-dependent signatures. At present, the products of water dissociation on TiO_2(110) have been fully characterized and understood. However, as this particular surface continues to be explored for the production of hydrogen via photocatalytic water splitting, the results reported here can stimulate new avenues to understand more complex adsorbates (e.g., alcohols)[18,39,40] acting as electron donors/hole traps and their bias-dependent STM signatures.

AUTHOR INFORMATION

Corresponding Author

*E-mail: cciobanu@mines.edu.

ORCID

Peter Sutter: 0000-0002-3301-309X

Cristian V. Ciobanu: 0000-0002-8476-4467

Notes

The authors declare no competing financial interest.

ACKNOWLEDGMENTS

The calculations were performed at the high-performance computing clusters of the Golden Energy Computing Organization at Colorado School of Mines.

REFERENCES

(1) Linsebigler, A. L.; Lu, G.; Yates, J. T. Photocatalysis on TiO2 Surfaces: Principles, Mechanisms, and Selected Results. *Chem. Rev.* **1995**, *95*, 735−758.

(2) Guo, Q.; Zhou, C.; Ma, Z.; Ren, Z.; Fan, H.; Yang, X. Elementary photocatalytic chemistry on TiO2 surfaces. *Chem. Soc. Rev.* **2016**, *45*, 3701−3730.

(3) Rodriguez, J. A.; Ma, S.; Liu, P.; Hrbek, J.; Evans, J.; Perez, M. Activity of CeOx and TiOx nanoparticles grown on Au(111) in the water-gas shift reaction. *Science* **2007**, *318*, 1757−1760.

(4) Grätzel, M. Photoelectrochemical cells. *Nature* **2001**, *414*, 338−344.

(5) Feng, X.; Shankar, K.; Varghese, O. K.; Paulose, M.; Latempa, T. J.; Grimes, C. A. Vertically Aligned Single Crystal TiO2Nanowire Arrays Grown Directly on Transparent Conducting Oxide Coated Glass: Synthesis Details and Applications. *Nano Lett.* **2008**, *8*, 3781−3786.

(6) Savage, N.; Chwieroth, B.; Ginwalla, A.; Patton, B. R.; Akbar, S. A.; Dutta, P. K. Composite n-p semiconducting titanium oxides as gas sensors. *Sens. Actuators, B* **2001**, *79*, 17−27.

(7) Diebold, U. The surface science of titanium dioxide. *Surf. Sci. Rep.* **2003**, *48*, 53−229.

(8) Bikondoa, O.; Pang, C. L.; Ithnin, R.; Muryn, C. A.; Onishi, H.; Thornton, G. Direct visualization of defect-mediated dissociation of water on TiO2(110). *Nat. Mater.* **2006**, *5*, 189−192.

(9) Diebold, U.; Anderson, J. F.; Ng, K.-O.; Vanderbilt, D. Evidence for the tunneling site on transition-metal oxides: TiO2(110). *Phys. Rev. Lett.* **1996**, *77*, 1322−1325.

(10) Schaub, R.; Thostrup, P.; Lopez, N.; Lægsgaard, E.; Stensgaard, I.; Nørskov, J. K.; Besenbacher, F. Oxygen vacancies as active sites for water dissociation on rutile TiO_2(110). *Phys. Rev. Lett.* **2001**, *87*, 266104.

DOI: 10.1021/acsomega.8b01056
ACS Omega 2018, 3, 6540−6545

(11) Diebold, U.; Lehman, J.; Mahmoud, T.; Kuhn, M.; Leonardelli, G.; Hebenstreit, W.; Schmid, M.; Varga, P. Intrinsic defects on a TiO2(110)(1×1) surface and their reaction with oxygen: a scanning tunneling microscopy study. *Surf. Sci.* **1998**, *411*, 137−153.
(12) Wendt, S.; Schaub, R.; Matthiesen, J.; Vestergaard, E. K.; Wahlström, E.; Rasmussen, M. D.; Thostrup, P.; Molina, L. M.; Lægsgaard, E.; Stensgaard, I.; Hammer, B.; Besenbacher, F. Oxygen vacancies on TiO2(110) and their interaction with H2O and O2: A combined high-resolution STM and DFT study. *Surf. Sci.* **2005**, *598*, 226−245.
(13) Suzuki, S.; Fukui, K.-i.; Onishi, H.; Iwasawa, Y. Hydrogen Adatoms onTiO2(110)−(1×1)Characterized by Scanning Tunneling Microscopy and Electron Stimulated Desorption. *Phys. Rev. Lett.* **2000**, *84*, 2156−2159.
(14) Di Valentin, C.; Pacchioni, G.; Selloni, A. Electronic structure of defect states in hydroxylated and reduced rutile TiO_2(110) surfaces. *Phys. Rev. Lett.* **2006**, *97*, 166803.
(15) Teobaldi, G.; Hofer, W. A.; Bikondoa, O.; Pang, C. L.; Cabailh, G.; Thornton, G. Modelling STM images of TiO2(110) from first-principles: Defects, water adsorption and dissociation products. *Chem. Phys. Lett.* **2007**, *437*, 73−78.
(16) Sánchez-Sánchez, C.; González, C.; Jelinek, P.; Méndez, J.; de Andres, P. L.; Martín-Gago, J. A.; López, M. F. Understanding atomic-resolved STM images on TiO2(110)-(1 × 1) surface by DFT calculations. *Nanotechnology* **2010**, *21*, 405702.
(17) Di Valentin, C. Scanning tunneling microscopy image simulation of the rutile (110) TiO2 surface with hybrid functionals and the localized basis set approach. *J. Chem. Phys.* **2007**, *127*, 154705.
(18) Zhang, W.; Li, Z.; Wang, B.; Yang, J. Scanning tunneling microscopy and density functional theory combined studies of rutile TiO2(1 1 0) surface chemistry: Watch surface processes at the atomic scale. *Int. J. Quantum Chem.* **2013**, *113*, 89−95.
(19) Stroscio, J. A.; Feenstra, R. M.; Fein, A. P. Electronic Structure of the Si(111)2 × 1 Surface by Scanning-Tunneling Microscopy. *Phys. Rev. Lett.* **1986**, *57*, 2579−2582.
(20) Kwon, S.-Y.; Ciobanu, C. V.; Petrova, V.; Shenoy, V. B.; Bareño, J.; Gambin, V.; Petrov, I.; Kodambaka, S. Growth of semiconducting graphene on palladium. *Nano Lett.* **2009**, *9*, 3985−3990.
(21) Binnig, G.; Rohrer, H.; Gerber, C.; Weibel, E. 7 × 7 Reconstruction on Si(111) Resolved in Real Space. *Phys. Rev. Lett.* **1983**, *50*, 120−123.
(22) Kendrick, C.; LeLay, G.; Kahn, A. Bias-dependent imaging of the In-terminated InAs(001)(4×2)c(8×2)surface by STM: Reconstruction and transitional defect. *Phys. Rev. B: Condens. Matter Mater. Phys.* **1996**, *54*, 17877−17883.
(23) MacLeod, J. M.; Miwa, R. H.; Srivastava, G. P.; McLean, A. B. The electronic origin of contrast reversal in bias-dependent STM images of nanolines. *Surf. Sci.* **2005**, *576*, 116−122.
(24) Claypool, C. L.; Faglioni, F.; Goddard, W. A.; Gray, H. B.; Lewis, N. S.; Marcus, R. A. Source of image contrast in STM images of functionalized alkanes on graphite: A systematic functional group approach. *J. Phys. Chem. B* **1997**, *101*, 5978−5995.
(25) Kappes, B. B.; Maddox, W. B.; Acharya, D. P.; Sutter, P.; Ciobanu, C. V. Interactions of same-row oxygen vacancies on rutile TiO_2(110). *Phys. Rev. B: Condens. Matter Mater. Phys.* **2011**, *84*, 161402.
(26) Acharya, D. P.; Ciobanu, C. V.; Camillone, N.; Sutter, P. Mechanism of Electron-Induced Hydrogen Desorption from Hydroxylated Rutile TiO2 (110). *J. Phys. Chem. C* **2010**, *114*, 21510−21515.
(27) Cortés, R.; Acharya, D. P.; Ciobanu, C. V.; Sutter, E.; Sutter, P. Graphene on Ru(0001) Moiré Corrugation Studied by Scanning Tunneling Microscopy on Au/Graphene/Ru(0001) Heterostructures. *J. Phys. Chem. C* **2013**, *117*, 20675−20680.
(28) Perdew, J. P.; Burke, K.; Ernzerhof, M. Generalized gradient approximation made simple. *Phys. Rev. Lett.* **1996**, *77*, 3865−3868.
(29) Kresse, G.; Furthmüller, J. Efficiency of ab-initio total energy calculations for metals and semiconductors using a plane-wave basis set. *Comput. Mater. Sci.* **1996**, *6*, 15−50.
(30) Kresse, G.; Furthmüller, J. Efficient iterative schemes forab initiototal-energy calculations using a plane-wave basis set. *Phys. Rev. B: Condens. Matter Mater. Phys.* **1996**, *54*, 11169−11186.
(31) Kresse, G.; Joubert, D. From ultrasoft pseudopotentials to the projector augmented-wave method. *Phys. Rev. B: Condens. Matter Mater. Phys.* **1999**, *59*, 1758−1775.
(32) Dudarev, S. L.; Botton, G. A.; Savrasov, S. Y.; Humphreys, C. J.; Sutton, A. P. Electron-energy-loss spectra and the structural stability of nickel oxide: An LSDA+U study. *Phys. Rev. B: Condens. Matter Mater. Phys.* **1998**, *57*, 1505−1509.
(33) Morgan, B. J.; Watson, G. W. A DFT+U description of oxygen vacancies at the TiO2 rutile (110) surface. *Surf. Sci.* **2007**, *601*, 5034−5041.
(34) Henrich, V. E.; Dresselhaus, G.; Zeiger, H. J. Observation of Two-Dimensional Phases Associated with Defect States on the Surface of TiO2. *Phys. Rev. Lett.* **1976**, *36*, 1335−1339.
(35) Tersoff, J.; Hamann, D. R. Theory of the scanning tunneling microscope. *Phys. Rev. B: Condens. Matter Mater. Phys.* **1985**, *31*, 805−813.
(36) Göpel, W.; Anderson, J. A.; Frankel, D.; Jaehnig, M.; Phillips, K.; Schäfer, J. A.; Rocker, G. Surface defects of TiO2(110): A combined XPS, XAES AND ELS study. *Surf. Sci.* **1984**, *139*, 333−346.
(37) Rocker, G.; Schaefer, J. A.; Göpel, W. Localized and delocalized vibrations onTiO2(110) studied by high-resolution electron-energy-loss spectroscopy. *Phys. Rev. B: Condens. Matter Mater. Phys.* **1984**, *30*, 3704−3708.
(38) Minato, T.; Sainoo, Y.; Kim, Y.; Kato, H. S.; Aika, K.-i.; Kawai, M.; Zhao, J.; Petek, H.; Huang, T.; He, W.; Wang, B.; Wang, Z.; Zhao, Y.; Yang, J.; Hou, J. G. The electronic structure of oxygen atom vacancy and hydroxyl impurity defects on titanium dioxide (110) surface. *J. Chem. Phys.* **2009**, *130*, 124502.
(39) Alghamdi, H.; Idriss, H. Study of the modes of adsorption and electronic structure of hydrogen peroxide and ethanol over TiO 2 rutile (110) surface within the context of water splitting. *Surf. Sci.* **2018**, *669*, 103−113.
(40) Zheng, Q.; Tan, S.; Feng, H.; Cui, X.; Zhao, J.; Wang, B. Dynamic Equilibrium of Reversible Reactions and Migration of Hydrogen Atoms Mediated by Diffusive Methanol on Rutile TiO2 (110)-(1 × 1) Surface. *J. Phys. Chem. C* **2016**, *120*, 7728−7735.

DOI: 10.1021/acsomega.8b01056
ACS Omega 2018, 3, 6540−6545